Energy and symmetry of self-assembled two-dimensional dipole clusters in magnetic confinement

M. Golosovsky,* Y. Saado, and D. Davidov

The Racah Institute of Physics, The Hebrew University of Jerusalem, Jerusalem 91904, Israel
(Received 27 July 2000; revised manuscript received 29 January 2002; published 12 June 2002; publisher error corrected 26 June 2002)

We report on confined two-dimensional (2D) dipole clusters formed by small ferromagnetic particles floating at the liquid-air interface and confined by nonuniform external magnetic field. The particles self assemble into hexagonally ordered clusters whose lattice constant can be magnetically tuned. We study the area S, the energy E, the chemical potential μ, and the lattice constant a, of 2D clusters as functions of particle number N for $N < 130$. We develop a continuum approximation which accounts fairly well for the smooth part of $\mu(N)$, $S(N)$, and $a(N)$ dependences. In addition to these dependences, we observe quasiperiodic fluctuations with dips at "magic" numbers corresponding to particularly symmetric particle configurations. We demonstrate that these fluctuations are related to the cluster symmetry and to the cluster center of mass position.

I. INTRODUCTION

Artificial crystals draw much attention as model systems by which to study quantum dots [1], quantum dot arrays, melting, crystallization, and lattice defects [2–8,10]. They can be fabricated step by step or can be formed spontaneously in the system of interacting particles, such as superparamagnetic particles in fluids [9,10], charged dust particles in plasma [11], vortices [12,13], electrons on surface of the liquid helium [14], etc. Recently, artificial crystals have attracted much interest due to their potential application as photonic band-gap materials [15]. In this context, self-assembled structures resulting from van der Waals, capillary [16], electric [8], and magnetic [3–6,9,17–19] interactions are promising. An important issue here is tunability which can be achieved through external fields. In particular, a magnetic field can rotate the particles [20,21], and affect crystal symmetry [19] or the lattice constant [10,18,22].

Self-assembly driven by magnetic forces can be realized in the system of magnetic particles at the air-liquid interface (interfacial colloidal crystals) [23] or in the bulk of the liquid (ferrofluids). The particles in ferrofluids self-assemble into nonperiodic three-dimensional (3D) patterns [24] and are less promising as photonic crystals. Magnetic particles at the liquid-air interface form 2D periodically ordered clusters and thus are much more promising as photonic crystals. Although floating superparamagnetic particles have been used for studies of 2D melting [4,5], floating ferromagnetic particles were used to demonstrate magnetic interactions [9,25,26] and vortices in superconductors [27], application of floating ferromagnetic particles for tunable photonic crystal is quite novel. We have recently built a photonic crystal using a stack of 2D self-assembled arrays of ferromagnetic particles on liquid interface with magnetic-field-dependent lateral lattice constant [18], and observed a tunable photonic stop band in the microwave range [22]. This raises an interesting question of what determines the structure, size, and lattice constant of the clusters of magnetic particles. In this paper, we study experimentally and theoretically 2D clusters of macroscopic

ferromagnetic particles on a stationary liquid surface in a magnetic confinement. We explore the dependence of their thermodynamic properties such as area, lattice constant, energy, and chemical potential on particle number. We show an interesting interplay between continuum and discrete properties of these clusters. This is an interesting example of soft condensed matter in confined geometry and under external field.

II. EXPERIMENTAL PROCEDURE AND PROCESSING OF THE RESULTS

Our experimental setup has been designed to represent as closely as possible the generic system of interacting dipoles in a parabolic confinement. The "dipoles" are Nd-Fe-B ferromagnetic disks (Fig. 1) encapsulated within a light material floating on the liquid (water, decane, etc.). Particle magnetic moments are perpendicular to the liquid interface, so the particles repel each other and self-assemble into hexagonally ordered clusters which, in the absence of an external magnetic field, fill the whole container. The liquid serves two goals: (i) lubrication—to allow self-assembly driven by weak lateral forces, and (ii) stabilization against the flip. A container with the particles and liquid is encircled by a current-carrying coil (radius $r_c = 45$ cm, height 5 cm, number of turns $N_t = 127$) which provides an inhomogeneous magnetic field in which to confine particles together and to vary the size and the lattice constant of the resulting cluster. The magnetic field of the coil is [28]
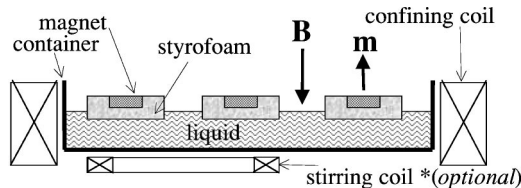
FIG. 1. Experimental setup. Small permanent magnets encapsulated within styrofoam disks float on the surface of the water. They repel each other and are confined within a nonuniform magnetic field produced by an external coil. Container diameter is 90 cm, magnet diameter is 5 mm, float diameter is 2.5 cm.

*Email address: golos@vms.huji.ac.il

$$B(r) = \frac{\mu_0 I N_t}{2\pi} \left(\frac{K_{el}}{r_c - r} + \frac{E_{el}}{r_c + r} \right), \tag{1}$$

where I is the current, $K_{el}(k)$ and $E_{el}(k)$ are elliptical integrals of the first and second kind, and $k^2 = 4 r_c r / (r_c + r)^2$. For $r < 0.9 r_c$, Eq. (1), with an accuracy of 2.5%, can be approximated by

$$B \approx B_0 \left(1 + 0.75 \frac{r^2}{r_c^2 - r^2} \right), \tag{2}$$

where $B_0 = \mu_0 I N_t / 2 r_c$ is the field in the center of the coil. For $r \ll r_c$, Eq. (1) reduces to parabolic dependence $B \sim r^2$.

In a moderate external magnetic field the particles are oriented in such a way that their magnetic moments are parallel to each other and perpendicular to the liquid surface. At higher fields the particles become spontaneously tilted and the cluster splits into a few domains with different orientation of the particle magnetic moment with respect to the vertical. This resembles the smectic-A–smectic-C phase transition in liquid crystals. At even higher fields, flip instability occurs, the tilt angle becomes 90°, and the cluster collapses. This limits the range of magnetic fields that can be used for such confinement.

The particle configuration is determined by the radially dependent part of the Hamiltonian which, for macroscopic particles at ambient temperature, reduces to the sum of the pair interaction energy and the field energy,

$$H = E_{int} + E_{field} = \frac{\mu_0}{4\pi} \sum_{i<j} \frac{m_i m_j}{|r_i - r_j|^3} + \sum_{i=1}^{N} m_i B(r_i). \tag{3}$$

Here, m_i and r_i are particle magnetic moment and position, respectively. Generally, Eq. (3) allows us to find the energy for known particle positions. This tedious task is facilitated by the following analysis. For identical particles we introduce distance scale and energy scale,

$$r_0 = \left(\frac{\mu_0 m}{3\pi B_0} \right)^{1/5}, \quad E_0 = \frac{\mu_0 m^2}{4\pi r_0^3}, \tag{4}$$

and recast Eq. (3) in dimensionless form

$$E = E_{int} + E_{field} = \sum_{i<j} \frac{1}{|r_i - r_j|^3} + \sum_{i=1}^{N} \frac{r_i^2}{1 - \frac{r_i^2}{r_c^2}}, \tag{5}$$

where r_i and r_c are dimensionless parameters. Note that the lattice constant a scales with r_0. For superparamagnetic particles r_0 is field independent, since $m/B_0 = $ const. Conversely, for ferromagnetic particles with $m = $ const, the lattice constant is field dependent: $a, r_0 \sim B_0^{-1/5}$ [18]. That is why ferromagnetic particles may be more advantageous in the field of tunable photonic crystals than superparamagnetic particles [4,5,10,17].

Our goal is to find cluster energy for known particle positions. To this end we further simplify Eq. (5). We consider

δE, the energy deviation upon small uniform deformation $r_i \to \tilde{r}_i (1 + u)$, where $u \ll 1$ and $\tilde{r}_i$ is the equilibrium particle position. In the equilibrium state the linear term in δE vanishes, leading to

$$-3u\tilde{E}_{int} + 2u \sum_{i=1}^{N} \frac{\tilde{r}_i^2}{\left(1 - \frac{\tilde{r}_i^2}{r_c^2} \right)^2} = 0, \tag{6}$$

where $\tilde{E}$ is the energy in the equilibrium. Therefore,

$$\tilde{E}_{int} = \frac{2}{3} \sum_{i=1}^{N} \frac{\tilde{r}_i^2}{\left(1 - \frac{\tilde{r}_i^2}{r_c^2} \right)^2} \tag{7}$$

and Eq. (5) reduces to

$$\tilde{E} = \sum_{i=1}^{N} \frac{\tilde{r}_i^2}{1 - \frac{\tilde{r}_i^2}{r_c^2}} \left(1 + \frac{2/3}{1 - \frac{\tilde{r}_i^2}{r_c^2}} \right). \tag{8}$$

While Eq. (5) allows us to find energy by summation of N^2 terms, Eq. (8) contains only N terms and is less demanding with respect to accuracy of the experimentally determined particle positions. However, Eq. (8) strongly relies on the dipole-dipole interaction law, $E_{int} \sim 1/r^3$. Since we operate with finite-size particles, while Eq. (3) assumes point dipoles, the validity of Eq. (3) should be verified. Indeed, interaction energy of two parallel axially magnetized disks (diameter $D = 5$ mm, height $h = 2$ mm) situated at the distance $r \sim 3$–7 cm ($r \gg D, h$) is $E_{int} = (\mu_0 m^2 / 4\pi r^3)(1 + 3D^2/8r^2 - h^2/4r^2 \cdots)$. In our case, the second term in the brackets contributes $\sim 1\%$, the third term contributes $\sim 0.1\%$. Contribution of weak attractive capillary forces is also very small (0.1%), therefore, Eq. (8) is valid within 1%.

We focus here on the dependence of cluster parameters on the number of particles. We varied the particle number by adding/removing a particle at the cluster boundary, and then measured particle positions in the equilibrium. To accelerate equilibration we applied ''stimulated annealing;'' in other words, we stirred the particles using an oscillating magnetic field (Fig. 1) with slowly decreasing amplitude. After several minutes of stirring and subsequent relaxation, the particles self-assemble into a well-ordered cluster with a quite reproducible configuration which remains stable for several days. We maintained constant external field $B_0 = 0.6$ mT, at which the spontaneous tilt is absent, took the image of the cluster, and determined equilibrium particle positions. Then we calculated the energy using Eq. (8). The repeatability of energy determination is ~ 0.1–0.2 %. This was deduced from several experiments with the same cluster which was shaken between the measurements and then allowed to relax. (This procedure sometimes results in a slightly different cluster configuration, i.e., metastable states do occur. However, the difference in energy between these states does not exceed $\sim 0.15\%$.) With known energy we find the chemical poten-

(a) N=31   **(b) N=37**

(c) N=70   **(d) N=85**
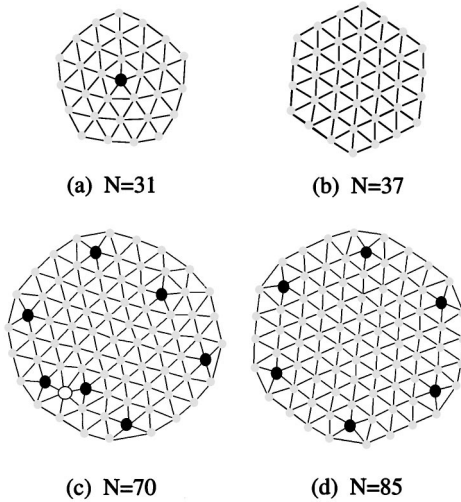
FIG. 2. Cluster images with superimposed Delaunay triangulation. Gray circles stand for normal coordination number ($Z=6$), filled circles stand for $Z=5$ (positive disclination), and open circles stand for $Z=7$ (negative disclination). (a) $N=31$—note pentagonal faceting; (b) $N=37$—a perfect hexagonal packing. Note faceting and absence of defects; (c) $N=70$—an ordinary cluster. Note a dislocation (5–7 pair) attached to a disclination; (d) $N=85$—a "magic" cluster. Note hexagonal structure, circular shape, and six topological disclinations close to the edge.

tial, $\mu = \partial E / \partial N = E(N) - E(N-1)$. We calculate the scale r_0 [Eq. (4)] from the interparticle distances in small clusters (2–7 particles) whose configurations are obvious, and find $r_0 = 7.05$ cm. This yields a particle magnetic moment of $m = 38$ emu, which is consistent with the saturation magnetization of Nd-Fe-B ($\mu_0 M = 1.22$ T). The energy scale [Eq. (4)] is $E_0 = 0.41$ μJ. We perform Voronoi construction on the cluster image and find cluster area, S. This can be defined as the sum of areas of Voronoi polyedra, or as $S = \pi D^2/4$ where D is the cluster diameter. The areas calculated according to these two definitions differ by 3.5%, so we adopted an intermediate definition $S = \pi R^2$ where R is the *average* cluster radius. Delauney triangulation allows one to find cluster perimeter P and the number of particles at the periphery N_p. The lattice constant at the edge is found from $a_{edge} = P/N_p$. The lattice constant in the center, a_0, is determined as the average nearest-neighbor distance for the particle which is the closest to the center of the potential ($r=0$).

III. EXPERIMENTAL RESULTS AND COMPARISON TO THE MODEL

Figure 2 shows images of several clusters. The clusters with small N acquire very different forms and can even have pentagonal faceting [Fig. 2(a)], which is usually associated with quasicrystals [19]. At higher N, the particles are arranged into an almost perfect hexagonal lattice. For small N, corresponding to perfect hexagonal packing, the cluster acquires a hexagonal shape [Fig. 2(b)]; for bigger N, the cluster tends to acquire a circular shape [Fig. 2(c)], which inevitably results in deviations from the perfect hexagonal order. The deviations are of two kinds: elastic strain and defects. Elastic
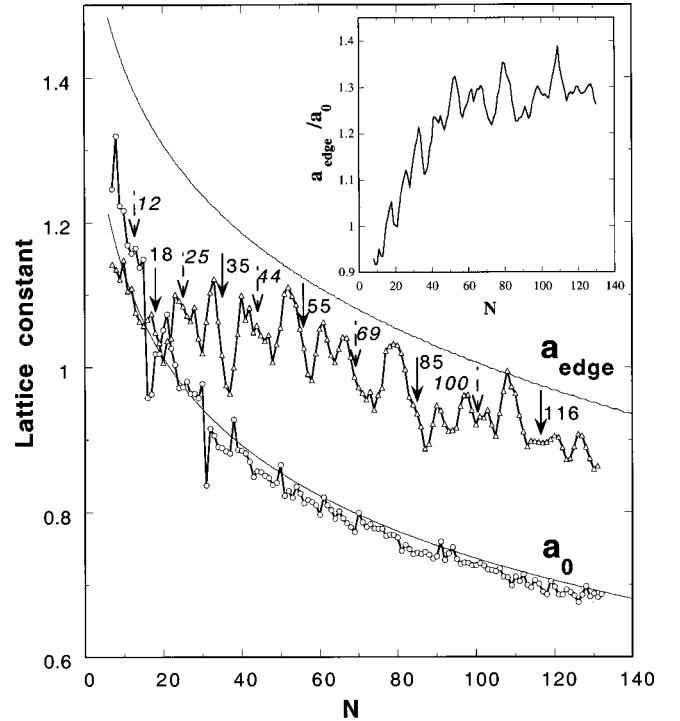
FIG. 3. The lattice constant in the center a_0 and at the cluster edge a_{edge} (in dimensionless units). The inset shows their ratio. Continuous lines show prediction of the continuum model (Appendix). Continuous arrows show magic numbers (primary series) and dashed arrows show the secondary series. The magic numbers strongly correlate with the local minima in $a_{edge}(N)$.

strain results primarily from the radial density variation. Indeed, Fig. 3 shows that the lattice constant in the center a_0 is lower than the lattice constant at the edge a_{edge}. The ratio a_{edge}/a_0 slowly increases with N and for $N>50$ is ~ 1.28 (Fig. 3, inset). The average strain associated with this lattice-constant variation is $u \sim (a_{edge} - a_0)/R \sim 4$–$5$ %. Actually, the strain is much smaller in the center and increases towards the edges. When the strain exceeds the elastic limit (~ 10–15 %) the defects (dislocations and disclinations [6]) are formed. Apart from six topological disclinations which are present in all circular-shaped clusters [Figs. 2(c) and 2(d)] due to competition between the hexagonal ordering and circular-symmetric confinement [1], many clusters contain one or few dislocations [Fig. 2(c)]. The dislocations and disclinations usually reside in the vicinity of the cluster edge, while the central part of the cluster can be made free of defects. Figure 4 shows the number of dislocations in different clusters. For $N<110$ there are clusters without dislocations or with 1–2 dislocations. For $N>110$, dislocation density dramatically increases. Numerical simulations of Ref. [1] for 2D Coulomb clusters in a parabolic confinement also suggest a dramatic increase in dislocation density for $N >140$.

In what follows, we study the dependence of the cluster properties on particle number. Figure 5 shows almost monotonic dependences of the area and chemical potential on particle number with some fluctuations. To analyze the smooth part of these dependences we develop a continuum model
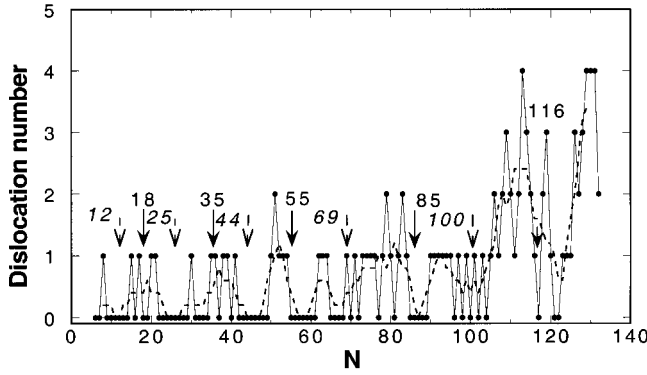
FIG. 4. The number of dislocations in the 2D clusters as a function of particle number N. Dashed line shows exact data, continuous line is obtained after smoothing. Continuous arrows show magic numbers (primary series) and dashed arrows show the secondary series. The magic numbers correlate with the minimum number of dislocations.

and calculate total cluster energy by replacing the sum [Eq. (5)] by the integral over the cluster area. The simplest approximation assuming constant particle density ρ and parabolic confinement yields

$$E=\int_a^R \rho\left(\frac{1}{2r^3}+r^2\right)ds\cong N\left(\frac{4}{a^3}+\frac{R^2}{2}\right). \quad (9)$$

Here, R is the cluster radius, a is the lattice constant, and $\rho\approx 4/\pi a^2$. The first term in Eq. (9) represents E_{int}, while the second term represents E_{field}. For parabolic confinement their ratio is 2:3 [this can be obtained from Eq. (6) by setting $r_c\rightarrow\infty$], hence, Eq. (9) yields $16/a^3=3R^2$. Combining it with the obvious relation, $R\approx aN^{1/2}/2$, we find

$$R=\left(\frac{3}{2}\right)^{1/5}N^{3/10}, \quad a_a=\left(\frac{48}{N}\right)^{1/5}, \quad E\sim 0.98N^{8/5},$$

$$\mu\sim 1.57N^{3/5}, \quad S\sim 3.69N^{3/5}, \quad K\sim 1.59N, \quad (10)$$

where $K=\partial E/\partial S$ is the bulk compression modulus. Equation (10) (dash-dotted line in Fig. 5) underestimates the chemical potential for $N>20$ and does not account for the radial density gradient which is clearly observed in Fig. 3 (the difference between a_0 and a_{edge}). A more elaborate model (Appendix) takes into account (i) spatial variation of the density, (ii) surface tension, and (iii) deviation of the potential from parabolicity. This model results in an algebraic equation [Eq. (A17), Appendix] for the spatially dependent density which is solved numerically for a given potential and yields $a(N)$, $S(N)$, and $\mu(N)$. This model, with confining potential given by Eq. (2), fits fairly well the experimentally found $S(N)$ and $\mu(N)$ (solid lines in Fig. 5). Systematic deviations at small N are expected and arise from the inadequacy of the continuum approach when only a few particles are present. Figure 3 shows the prediction of this model for the lattice
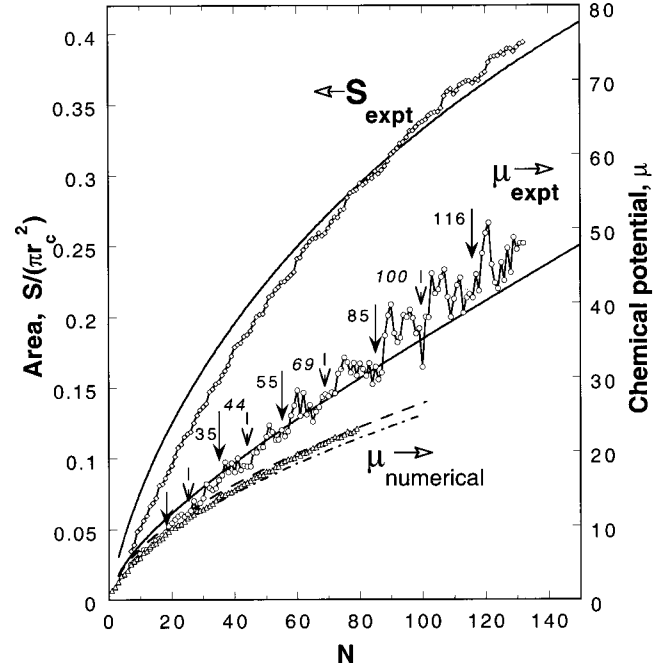
FIG. 5. Cluster area S (normalized to coil area) and chemical potential μ [in the units of E_0, see Eq. (4)] as functions of particle number N. The circles stand for experimental data (smoothed). The triangles show results of numerical simulation [29] for the dipoles in a parabolic confinement. The dash-dotted line shows prediction of a simplified model [Eq. (10)] assuming constant density. The dashed line shows our model prediction (Appendix) for the parabolic confinement $B\sim r^2$ and varying density. The solid lines show our model predictions (Appendix) for the confining field $B\sim r^2/(1-r^2)$ which has been used in our experiment. Note the good correspondence between the experimental results and the model, as well as between the numerical results and the corresponding model prediction. Continuous arrows show magic numbers (primary series) and dashed arrows show the secondary series. The magic numbers approximately correspond to the centers of plateaus in μ_{expt}.

constant. The lattice constant in the center is accounted for fairly well, while the lattice constant at the cluster edge is slightly overestimated.

Since the parabolic confining potential is quite general, it is important to check how deviation from parabolicity affects cluster structure. We compare our experiment results (Fig. 5, circles) for the dipole cluster in *almost parabolic confinement* [Eq. (2)] to numerical simulations of the dipole cluster in strictly *parabolic* confinement [29] (Fig. 5, triangles). For $N<20$ the chemical potential μ_{expt} almost coincides with the results of numerical simulations μ_{num}, while for $N>20$, $\mu_{expt}>\mu_{num}$. This is expected since for small N the particles are close to the center of the coil where the potential is very close to parabolic, while at bigger N more particles are in the area where the potential is more rigid than parabolic. Therefore, deviation of the confining potential [Eq. (2)] from parabolicity is important.

Deviations from the smooth dependence. Note fluctuations on top of smooth dependences $S(N)$ and $\mu(N)$ (Fig. 5) which at first glance look like noise. Nevertheless, these fluctuations are quite reproducible, since they are a direct con-

sequence of the crystalline order in the cluster. We find similar fluctuations in three experimental runs. These fluctuations appear in all cluster properties and are very prominent in μ, where they amount to 8%. Note regions in which μ and S hardly change upon the addition of new particles. Corresponding clusters are more dense, more symmetric, and have lower energy. Any deviation from high symmetry is accompanied by energy and area increase.

Although the deviations from the perfect symmetry can be quantified using continuous symmetry measure [32], we apply here an approach of Koulakov and Shklovskii [1], who numerically studied the particles with Coulomb/hard-sphere interaction in the parabolic confinement, and showed that the position of the cluster center of mass with respect to the unit cell may serve as an indicator of a deviation from the perfect symmetry. Reference [1] demonstrated that while the absolute position of the cluster center of mass is always at the minimum of the external potential, its position in the unit cell is preferably located at high symmetry points [for a hexagonal lattice these are points (A), (B), and (C)—see Fig. 6]. We measured distribution of the center-of-mass positions in the unit cell of our 2D dipole clusters and indeed found that it is strongly peaked at positions (A), (B), and (C) (Fig. 6, upper panel). The middle panel in Fig. 6 shows N_{cm}, a number of nearest neighbors at the center-of-mass position, as a function of particle number. [We take one of the points (A), (B), or (C) which is the closest to the center of mass and assign $N_{cm}=6$ for (A), $N_{cm}=3$ for (B), and $N_{cm}=2$ for (C)]. We observe that (i) N_{cm} changes quasiperiodically in $N^{1/2}$, (ii) dependence N_{cm} vs N exhibits continuous regions where the center of mass resides in the position of sixfold symmetry (A), and (iii) pronounced dips in dS/dN occur in these regions. Shallow dips correspond to position (B). We define "magic" numbers as those corresponding to the middle points of the plateaus, where the center of mass resides in a high-symmetry point. The primary "magic" series $N_m \approx 18,35,55,85,116\cdots$ corresponds to the centers of the plateaus with $N_{cm}=6$ and a secondary "magic" series $N_m \approx 12,25,44,69,100\cdots$ corresponds to the centers of the plateaus with $N_{cm}=3$. The primary series may be approximated by empirical dependence $N_m \approx 1+2.75s(s-1); s=0,1,2\cdots$ which is related to the perfect hexagonal packing: $N=1 +3s(s-1); s=0,1,2\cdots$. The width of the plateaus approximately corresponds to one crystalline row, or $(N/3)^{1/2}$. The clusters with a "magic" or close to "magic" number of particles show almost perfect hexagonal packing and a minimum of defects (Fig. 4). Therefore, the center-of-mass position with respect to the unit cell is indeed a good indicator of cluster "quality."

IV. DISCUSSION AND CONCLUSIONS

In a broad context, dependence of the cluster properties on the number of particles (Figs. 3–6) reminds us of the Mendeleev table of elements, in particular, dependence of atomic radius and ionization potential on atomic number which also show quasiperiodic oscillations in addition to smooth dependences. Magic clusters are actually analogs of noble gases, while the continuum model (Appendix) is
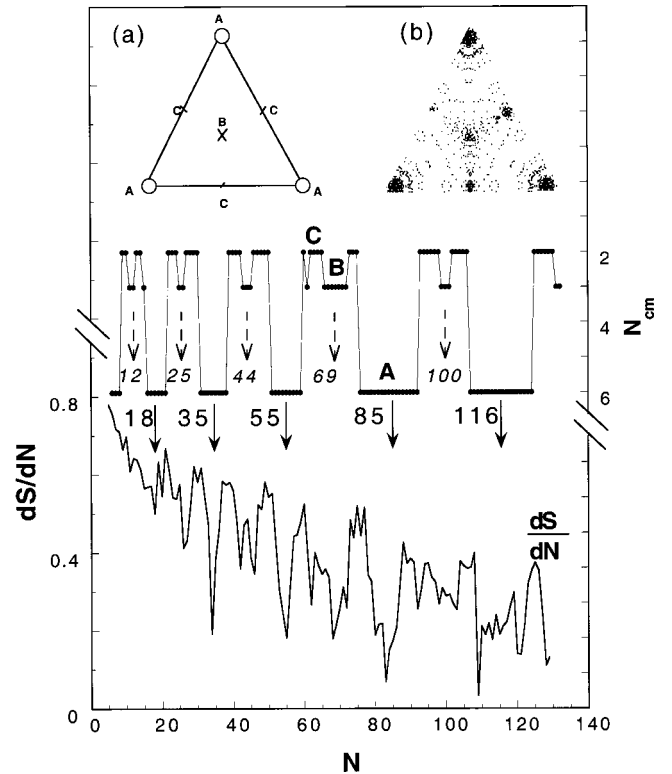
FIG. 6. Position of the cluster center of mass. Upper panel—(a) Unit cell and the positions of high symmetry, (A), (B), and (C). (b) Distribution of the center-of-mass positions in the unit cell. Each point corresponds to a cluster with a certain particle number N. Note that the center of mass sticks to positions (A), (B), and (C). The centers of wide plateaus corresponding to most symmetric clusters with $N_{cm}=6$ are denoted by continuous arrows and the corresponding "magic" numbers are shown. The centers of shallow plateaus corresponding to the clusters with $N_{cm}=3$ are denoted by dashed arrows and the corresponding secondary "magic" numbers are shown. Middle panel shows number of nearest-neighbors N_{cm} at the center-of-mass position. Lower panel shows dS/dN [in dimensionless units, see Eq. (4)]. The magic numbers correlate with the minima in dS/dN.

analogous to the Thomas-Fermi model for atoms. However, due to different dimensionality and interaction laws, the magic numbers are different. While magic numbers are well known for free-standing 3D clusters [30] and have been found in computer simulations for 2D clusters with various pair interaction laws [1,29,31], we are unaware of previous *experimental* observation of magic 2D clusters in a lateral confining field. The magic numbers in the system of few interacting particles are ubiquitous (chemical elements, nucleii, etc.) and usually related to the shell structure of these systems. The magic clusters are more stable, since they are highly symmetric and are characterized by local energy minimum. This is probably true for the systems entirely dominated by the potential energy, while in general, highly symmetric configurations do not necessarily have the lowest energy (spontaneous symmetry breaking).

Quasiperiodic fluctuations in cluster properties were found in numerical simulations for the particles with dipole [29], Coulomb, and hard-sphere [1] interactions. The value

of fluctuations depends on the pair interaction law, increasing with the rigidity of the interaction potential [1]. Most probably, the value of the fluctuations also depends on the confining potential. Anyway, fluctuations in μ that were found in numerical simulations for the dipole clusters in a parabolic potential [29] (Fig. 5, triangles) are smaller than those found in our experiments with the dipole clusters in a more rigid potential (Fig. 5, circles).

In what follows, we estimate the value of the fluctuations and the width of continuous regions in which the cluster configuration is particularly symmetric. Consider a magic cluster. Upon addition of new particles it undergoes energetically expensive elastic and plastic deformations in order to keep the center of mass at the position of high symmetry. This occurs until another position of high symmetry becomes energetically favorable. Upon further addition, a rearrangement of the whole cluster (avalanche) occurs whereby the center of mass moves to a large distance, of the order of a lattice-constant a. These avalanches are accompanied by fluctuations in cluster properties. Addition of new particles to a magic cluster does not lead to the center-of-mass displacement until approximately one crystalline row is added. If the cluster were incompressible, the area would increase by $\delta S \approx S \Delta N / N$. In reality, δS is smaller due to relaxation. In fact, immobility of the center of mass means that a highly symmetric cluster adopts new particles without appreciable increase in area, namely, $dS/dN \approx 0$. Indeed, our experimental observations show deep minima in dS/dN (Fig. 6). Corresponding deviation from the smooth dependence is thus $\delta S \approx s \Delta N$ where $s = (dS/dN)_{ave}$ is the area per particle and $\Delta N \approx (N/3)^{1/2}$ (one crystalline row). Since $s \approx 0.6S/N$ [Eq. (10)], then $\delta S \approx 0.6S/(3N)^{1/2}$. This fluctuation originates from the cluster relaxation which occurs via elastic and plastic deformations. If the deformation u were purely elastic, then $u = \delta S/2S$ and the corresponding variation of the energy or of the chemical potential is $\delta \mu = K S u^2/2 \approx 0.1 \, \mu$, where K is the bulk compression modulus. Experimentally observed fluctuations (0.1–$0.05 \, \mu$) are smaller due to plastic deformation (formation of dislocations).

We expect that the dislocations reside close to the cluster edge where the strain is maximum. This is confirmed by our experiments. With respect to dislocation arrangement in big clusters, Ref. [1] argues that the dislocations should aggregate into a grain-boundary concentric to the cluster outer shell, while Ref. [33] conjectures that the dislocations arrange into a lattice of their own. Which scenario holds in reality may depend on the specific form of (i) the pair interaction and (ii) the confining potential. Further experiments should clarify this issue.

In conclusion, we demonstrate self-assembled 2D dipole clusters with a magnetically tunable lattice constant. Experimentally found dependences of the cluster area, chemical potential, and lattice constant as functions of particle number are fairly well described by our continuum model. Quasiperiodic deviations from the smooth dependences $\mu(N)$ and $S(N)$ occur at certain magic numbers and correspond to especially symmetric cluster configurations. These magic clusters are characterized by higher stability, lower elastic strain, and small number of defects. Position of the cluster center of mass with respect to the unit cell is a good indicator of the cluster quality.

APPENDIX: CONTINUUM MODEL OF A 2D DIPOLE CLUSTER IN A PARABOLIC CONFINEMENT

Consider a planar assembly of identical magnetic dipoles with magnetic moment m oriented perpendicular to the plane. The dipoles repel each other and are confined by the inhomogeneous magnetic field with almost parabolic radial dependence $B = \alpha r^2 + \beta r^4 + \cdots$. The particle configuration is determined by the Hamiltonian which, for macroscopic particles at ambient temperature, reduces to potential energy

$$H = E_{int} + E_{field} = \frac{\mu_0}{4\pi} \sum_{i \neq j} \frac{m_i m_j}{2|r_i - r_j|^3} + \sum_i m_i B(r_i). \tag{A1}$$

The first term here is the pair interaction energy and the second term is the field energy. (The factor of 2 in the denominator of the first term appears because each particle is counted twice). The interplay between these two terms dictates particle arrangement. In a radially symmetric magnetic field the particles organize into an almost circular cluster centered at the minimum of the magnetic field. Circular symmetry of the interparticle interaction forces drives the particles into a mostly symmetric configuration, namely, hexagonal lattice, which is, however, distorted due to (i) competition between the circular-symmetric confinement and local hexagonal symmetry; (ii) gradient of confining forces. Our aim is to find the density, energy, and radius of the cluster as a function of the particle number N. To solve this problem, we develop a continuum model and find the relation between the energy and the density of the cluster by replacing the sums in [Eq. (A1)] by the integral. We find

$$E = \int_0^R (\epsilon_{int} + mB) \rho \, ds, \tag{A2}$$

where $\rho(r)$ is the particle density, R is the cluster radius, and

$$\epsilon_{int}(r) = \frac{\mu_0 m^2}{8\pi} \int_{a*}^R \frac{\rho(r') ds'}{|\mathbf{r} - \mathbf{r}'|^3} \tag{A3}$$

is the interaction energy per particle. In contrast to Coulomb clusters where pure continuum approach is possible [34], dipole-dipole interaction diverges at short distances, hence, we introduce the cutoff $a*$ distance. Since the main contri-

bution to the integral [Eq. (A3)] comes from the nearest neighbors where density is almost constant, we set $\rho(r') = \rho(r)$, perform integration, and find

$$\epsilon_{int}(r) = \frac{\mu_0 m^2 \rho}{8\pi}\left[\frac{2\pi}{a^*} - \frac{4RE_{el}(r/R)}{R^2 - r^2}\right]. \qquad (A4)$$

Here $E_{el}(k)$ is the elliptical integral of the second kind which for all our practical needs can be replaced by the polynomial approximation,

$$E_{el}(k) \approx \frac{\pi}{2}(1 - k^2) + k^2, \qquad (A5)$$

which is fairly good for $0 < k < 1$. The first term in Eq. (A4) is the interaction energy per particle in the infinite cluster, while the second term represents the finite-size effect or surface correction. The cutoff distance a^* is found from the comparison to the corresponding lattice sum for the 2D infinite hexagonal lattice of parallel dipoles. Reference [8] calculated this sum and found $\Sigma 1/r_i^3 = 11.033/a_0^3$, where a_0 is the lattice constant. The corresponding integral for an infinite cluster with constant density yields

$$\sum \frac{1}{r_i^3} \approx \int_{a^*}^{\infty} \frac{\rho(r')ds'}{|\mathbf{r}-\mathbf{r}'|^3} = 2\pi\frac{\rho}{a^*}. \qquad (A6)$$

Since for the hexagonal lattice $\rho = 8/3\sqrt{3}a_0^2$, $a^* \approx 0.88a_0 \approx 1.09\rho^{-1/2}$. Note that a^* depends on ρ.

Since the integral [Eq. (A3)] diverges also at the upper limit $r \rightarrow R$, we introduce another cutoff r^* which is determined from the comparison of Eq. (A4) to the lattice sum for a particle at the edge of an infinite half-plane, namely, $\Sigma 1/r_i^3 = 6.72/a_0^3$. Equation (A4) transforms into

$$\epsilon_{int}(r^*) = \frac{2\pi\rho}{a^*} - \frac{2\pi\rho}{R} - \frac{4r^{*2}\rho}{R(R^2-r^{*2})}, \qquad (A7)$$

which results in implicit dependence

$$r^* \approx R - 0.82a^*(r^*). \qquad (A8)$$

The hydrostatic pressure is found from $p = -\partial\epsilon_{int}/\partial V$ which in 2D reduces to $p = -\partial\epsilon_{int}/\partial s = \rho^2\partial\epsilon_{int}/\partial\rho$ where s is the area per particle. Equation (A4) yields the equation of state

$$p = \frac{\mu_0 m^2}{4\pi}\left[1.38\pi\rho^{5/2} - \frac{2R\rho^2 E_{el}(r/R)}{R^2-r^2}\right]. \qquad (A9)$$

The density is found from the equation describing equilibrium of compressible solid under radial force [35]

$$\frac{\partial\sigma_r}{\partial r} + \frac{\sigma_r - \sigma_\Theta}{r} + \rho(r)\nabla U = 0. \qquad (A10)$$

Here, σ_r and σ_Θ are the radial and azimuthal components of the stress tensor. We express the stress σ through the hydrostatic pressure $p = (\sigma_r + \sigma_\Theta)/2$ and rewrite Eq. (A10) as

$$\frac{\nabla p}{\rho} + \frac{\nabla[r(\sigma_r - \sigma_\Theta)]}{2r\rho} + \nabla U = 0. \qquad (A11)$$

To solve Eq. (A11) we have to simplify the second term. For a particular case of incompressible (constant density) solid under parabolic potential [35], Eq. (A11) may be recast as

$$\frac{\nabla p}{\gamma\rho} + \nabla U = 0, \qquad (A12)$$

where

$$\gamma = (1 + 3\nu)/4, \qquad (A13)$$

ν is the Poisson ratio. The same Eq. (A12) holds for the liquid (even compressible) for which $\nu = 1$ and $\gamma = 1$. We assume that Eq. (A12), with γ given by Eq. (A13), holds also for our (compressible) dipole cluster. Results of Ref. [8] yield Poisson ratio for hexagonally ordered dipole cluster $\nu = 0.82$, hence, $\gamma = 0.865$.

Since the pressure is uniquely determined by density, the Eq. (A12) allows us to introduce the chemical potential μ $\nabla\mu = \nabla U + \nabla p/\gamma\rho$. We combine Eqs. (A9) and (A12) to find

$$\nabla\mu = m\nabla B + \frac{\mu_0 m^2}{4\pi\gamma}\left[2.29\pi\nabla(\rho^{3/2}) - \frac{2R}{\gamma\rho}\nabla\left(\frac{\rho^2 E_{el}(r/R)}{R^2-r^2}\right)\right], \qquad (A14)$$

where in the equilibrium $\nabla\mu = 0$. The different terms in Eq. (A14) may be estimated as follows. The first term in square brackets is the dominant one and represents the bulk internal energy. The second term represents surface correction and is smaller by a factor $a_0/R \ll 1$ everywhere except at the cluster edge. If the surface correction were totally negligible, then Eq. (A14) would yield a power-law dependence $\rho \sim (R^2 - r^2)^{2/3}$. We substitute this power-law dependence into Eq. (A14) and note that the last term may be represented as a gradient of some function

$$-\frac{1}{\rho}\nabla\left(\frac{\rho^2 E_{el}(r/R)}{R^2-r^2}\right) \approx \nabla\rho\left(\pi - \frac{r^2}{R^2-r^2}\right). \qquad (A15)$$

The elliptical integral has been replaced here by the polynomial approximation [Eq. (A5)]. We substitute Eq. (A15) into Eq. (A14), perform integration, and find

$$\mu = mB(r) + \frac{\mu_0 m^2}{4\pi\gamma}\left[2.29\pi\rho^{3/2} - \frac{2\pi\rho}{R} + \frac{2\rho r^2}{R(R^2-r^2)}\right]$$

$$= mB(R). \qquad (A16)$$

The first term in the square brackets is the elastic energy of compression and the last two terms represent surface tension.

To find the density we introduce dimensionless variables $z = (\pi R^2\rho)^{1/2}$, $x = r/R$, $b(x) = B(r)/B(R)$ and recast Eq. (A16) as follows:

$$1.29z^3 + 2z^2\left(\frac{x^2}{\pi(1-x^2)} - 1\right) - \gamma\left(\frac{R}{r_0}\right)^5 [1 - b(x)] = 0.$$
$$(A17)$$

Here, r_0 is the distance scale determined by the magnetic field [Eq. (4)]. We solve Eq. (A17) for given R, x, $b(x)$ and find $z(x,R)$, $\rho(x,R)$. The cutoff distance r^* is determined

from Eq. (A8) which reduces to $z^* = 4r^{*2}/(R^2 - r^{*2})$. Integration of the density yields the particle number

$$N(R) = \int_0^{r^*} \rho\,ds = 2\int_0^{x^*(R)} z^2(x,R)x\,dx \qquad (A18)$$

The function $N(R)$ is reverted resulting in an explicit dependence $R(N)$. The chemical potential is found from Eq. (A16).

[1] A. A. Koulakov and B. I. Shklovskii, Phys. Rev. B **57**, 2352 (1998).

[2] H. Loewen, J. Phys.: Condens. Matter **13**, R415 (2001).

[3] A. T. Skjeltorp, Phys. Rev. Lett. **51**, 2306 (1983).

[4] K. Zahn, R. Lenke, and G. Maret, Phys. Rev. Lett. **82**, 2721 (1999).

[5] R. Bubeck, C. Bechinger, S. Neser, and P. Leiderer, Phys. Rev. Lett. **82**, 3364 (1999).

[6] R. Seshadri and R. M. Westervelt, Phys. Rev. B **46**, 5142 (1992).

[7] I. V. Schweigert, V. A. Schweigert, and F. M. Peeters, Phys. Rev. Lett. **84**, 4381 (2000).

[8] R. E. Kusner, J. A. Mann, and A. J. Dahm, Phys. Rev. B **51**, 5746 (1995).

[9] B. A. Grzybowski, H. A. Stone, and G. W. Whitesides, Nature (London) **405**, 1033 (2000).

[10] X. L. Xu, G. Friedman, K. D. Humfeld, S. A. Majetich, and S. A. Asher, Adv. Mater. **13**, 1681 (2001).

[11] T. M. O'Neil, Phys. Today **52**, 24 (1999).

[12] L. J. Campbell and R. N. Ziff, Phys. Rev. B **20**, 1886 (1979).

[13] A. Geim, I. V. Grigorieva, S. V. Dubonos, J. G. S. Lok, J. C. Maan, A. E. Filippov, and F. M. Peeters, Nature (London) **390**, 259 (1997).

[14] C. C. Grimes and G. Adams, Phys. Rev. Lett. **42**, 795 (1979).

[15] J. D. Joannopoulos, R. D. Meade, and J. N. Winn, *Photonic Crystals* (Princeton University, Princeton, NJ, 1995).

[16] N. Bowden, A. Terfort, J. Carbeck, and G. M. Whitesides, Science **276**, 233 (1997).

[17] A. S. Dimitrov, T. Takahashi, K. Furusawa, and K. Nagayama, J. Phys. Chem. **100**, 3163 (1996); T. Takahashi, A. S. Dimitrov, and K. Nagayama, *ibid.* **100**, 3157 (1996).

[18] M. Golosovsky, Y. Saado, and D. Davidov, Appl. Phys. Lett.

75, 4168 (1999); Y. Saado, M. Golosovsky, D. Davidov, and A. Frenkel, Synth. Met. **116**, 427 (2001).

[19] W. J. Wen, L. Y. Zhang, and P. Sheng, Phys. Rev. Lett. **85**, 5464 (2000).

[20] B. Gates and Y. N. Xia, Adv. Mater. **13**, 1605 (2001).

[21] D. Lacoste, F. Donatini, S. Neveu, J. A. Serughetti, and B. A. Van Tiggelen, Phys. Rev. E **62**, 3934 (2000).

[22] Y. Saado, M. Golosovsky, D. Davidov, and A. Frenkel, Phys. Rev. B (to be published).

[23] H. Loewen, J. Phys.: Condens. Matter **13**, R145 (2001).

[24] P. G. de Gennes and P. A. Pincus, Phys. Kondens. Materie **11**, 189 (1970).

[25] P. Flanders, Am. J. Phys. **33**, 346 (1965).

[26] G. Schwarz, *Air Cushion Table Handbook*, PHYWE series of publications (Industrie-Druck GmbH, Gottingen, 1979).

[27] A. C. Rose-Innes and E. A. Stangham, Cryogenics **9**, 456 (1969).

[28] L. D. Landau, E. M. Lifshitz, and L. P. Pitaevskii, *Electrodynamics of Continuous Media* (Pergamon Press, London, 1984), Chap. 4.

[29] A. I. Belousov and Yu. E. Lozovik, Eur. Phys. J. D **8**, 251 (2000).

[30] T. P. Martin, Phys. Rep. **273**, 199 (1996).

[31] V. M. Bedanov and F. M. Peeters, Phys. Rev. B **49**, 2667 (1994).

[32] H. Zabrodsky, S. Peleg, and D. Avnir, J. Am. Chem. Soc. **114**, 7843 (1992).

[33] Y. V. Nazarov, Europhys. Lett. **32**, 443 (1996).

[34] I. N. Sneddon, *Mixed Boundary Value Problems in Potential Theory* (Wiley, New York, 1966).

[35] S. P. Timoshenko and J. N. Goodier, *Theory of Elasticity* (McGraw-Hill, New York, 1970).